Enhanced periodic modulation of electronic states in a hexagonal iron-nitride monolayer on Cu(001) via interfacial interaction

K. Ienaga,[1,*] T. Miyamachi,[1,†] Y. Takahashi,[1] N. Kawamura,[1,2] and F. Komori[1]
[1]*Institute for Solid State Physics, The University of Tokyo, Kashiwa, Chiba 277-8581, Japan*
[2]*Science and Technology Research Laboratories, NHK, Setagaya, Tokyo 157-8510, Japan*
(Received 31 May 2017; revised manuscript received 8 August 2017; published 28 August 2017)

Metal nitride has robust bonding between metal and nitrogen atoms. We have synthesized a monoatomic layer of a hexagonal-type iron nitride with strong Fe-N bond on the Cu(001) substrate with a fourfold lattice symmetry. From atomic-scale observation using scanning tunneling microscopy, we have found that the Fe-N film exhibits a strip structure consisting of regular and deformed hexagonal lattices. The lattices are deformed along a hypothetical Moiré pattern made by a perfect hexagonal lattice on the square Cu(001) lattice. With increasing the lattice deformation, the strain energy increases, whereas the periodic deformation of the Fe-N lattice can minimize the total lattice energy including the strain energy of the Fe-N in-plane bonding and interfacial bonding energy between the Fe-N layer and the Cu substrate. In dI/dV spectra, periodic spatial change of the unoccupied density of states due to the lattice strain was observed. This is attributed to an energy shift of the antibonding states due to compressive strain.

DOI: 10.1103/PhysRevB.96.085439

I. INTRODUCTION

Remarkable changes of electronic and magnetic properties have been reported in thin films from those in bulk crystals. In the case of a pseudomorphic film, the lattice constant is the same as that of the substrate because of the strong interfacial interaction, and the epitaxial strain is a crucial factor for these changes. Since the lattice of the overlayer is expanded or compressed, compared to that of the corresponding bulk crystal, its electronic states are strongly modified as in the case of axial pressure for the bulk. For example, the band gap increases with increasing orbital overlap by the lattice compression in semiconductor films [1–4]. In magnetic thin films, the easy-magnetization axis sometimes rotates during the pseudomorphic growths [5–7]. In contrast to these homogeneous changes, when the overlayer in-plane bonding is much stronger than the interfacial bonding with the substrate, the lattice mismatch between the overlayer and substrate just results in a nanometer-scale Moiré pattern. Even in this case, the local electronic states can change because the lattice relaxes to minimize the total strain energy [8,9]. Actually, the electronic states in the overlayers are often spatially modulated due to difference of local stacking or periodic displacement in the out-of-plane direction (e.g., corrugation or ripple) [9–16]. Thus, it is possible to modify the electronic and magnetic properties periodically in a nanometer scale by tuning the delicate balance between the in-plane and interfacial bonds.

In the present paper, we report an enhanced spatial modulation of the electronic structure in a monoatomic iron-nitride sheet on Cu(001) with periodic strain in a nanometer scale. Here, this system is suitable for realizing an intermediate situation between a strained epitaxial film and a quasi-free-standing atomic sheet. Transition-metal nitrides exhibit robust networks due to the covalent bond between nitrogen and metal atoms [17,18]. In the case of the monoatomic layers on the Cu substrates, they moderately interact with the substrate through the transition-metal 3d and N-p bonds [19,20]. Thus, formation of the monoatomic layers can be expected on a Cu substrate even with a different lattice symmetry.

Among various transition-metal nitrides, we have selected a Fe-N system, which contains various phases of different stoichiometries and crystal structures depending on an amount of N atoms [17,21]. One of the well-defined epitaxial films of iron nitrides is γ'-Fe_4N(001)/Cu(001) [22–25]. Another iron nitride that can grow on Cu(001) is the zinc-blend (ZnS) type FeN [26–28] because the interatomic distance of 2.56 Å in Cu(001) is quite close to an atomic row distance of 2.65 Å in the (111) plane of this crystal while the lattice symmetry is different. In this case, we can expect a hexagonal film stabilized by the Fe-N bond with a periodic nanopattern on the Cu(001) substrate with a fourfold symmetry. Indeed the similar example has been reported as a Cu_2N film with a square lattice on Cu(111) of threefold symmetry [29], although periodic shift in the electronic band structure is almost absent [30].

We have synthesized monoatomic films of a hexagonal-type iron nitride on Cu(001) and characterized them in an atomic scale using scanning tunneling microscopy/spectroscopy (STM/STS). In contrast to the well-known Fe_2N monoatomic films covering the terraces [22–25], the hexagonal films of iron nitride grow preferentially near step edges on the Cu(001) surface. To relax the strain due to the lattice mismatch at the interface, the hexagonal films show a striped nanopattern consisting of strained regions [8]. We demonstrate that the direction of the striped structure can be understood by a simple consideration starting from a Moiré pattern made by a hexagonal lattice on a square lattice. Formation of the resultant periodic superstructure is attributed to the strain-relief mechanism avoiding on-top stacking on the

*Present address: Department of Physics, Tokyo Institute of Technology, Meguro, Tokyo 152-8551, Japan, ienaga.k.aa@m.titech.ac.jp
†toshio.miyamachi@issp.u-tokyo.ac.jp

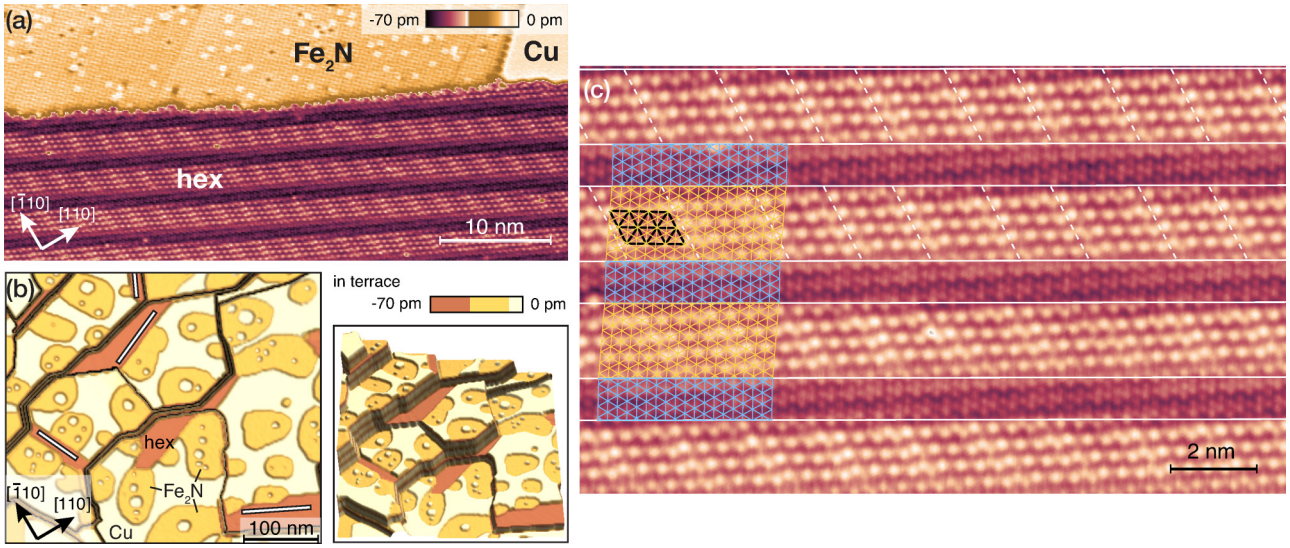

FIG. 1. Topographic images of iron nitride monoatomic layers on Cu(001). (a) Boundaries among Fe_2N, the striped hexagonal structure, and the bare Cu(001) within a single terrace at $I_t = 500$ pA, $V_b = -0.1$ V. (b) Top-view (left) and 3D (right) images of a wide area obtained at $I_t = 0.1$ nA, $V_b = 0.25$ V. The three regions are colored according to height difference within the same terrace. Solid white lines indicate four directions of the stripe structure. (c) Magnified image of a striped hexagonal region at $I_t = 0.5$ nA, $V_b = -0.1$ V. Solid white lines along the stripe direction divide the stripe structure into dark and bright areas, where blue and orange lattices are superimposed in the left side of the panel, respectively. The bright area contains protrusions corresponding to $(\sqrt{3}\times\sqrt{3})R30^\circ$-like superstructure as marked by black lines. The dashed white lines indicate phase boundaries of the superstructure, which repeat every three or four periods along the stripe direction.

substrate Cu(001) lattice. This indicates a significant interaction between the hexagonal-lattice overlayer and the substrate with a square lattice. We have revealed that the periodic strain strongly changes its local electronic structure using STM/STS.

II. EXPERIMENTAL SETUP

Iron nitride monoatomic layers were grown on a Cu(001) substrate in an ultrahigh vacuum chamber, from which the sample can be transferred *in situ* to an STM chamber. Base pressure of both chambers is below 1.0×10^{-10} Torr. First we prepared a clean and flat Cu(001) surface by several cycles of Ar^+ ion sputtering and annealing at 820 K. Then, nitrogen atoms were supplied to the clean surface by N^+ ion bombardment (0.5 keV) at room temperature (RT), and subsequently Fe was deposited on the surface at RT using an electron-bombardment type evaporator. Finally, the sample was annealed at 570 K for 15 min. Monoatomic films with a hexagonal atomic structure were formed near the step edges as well as the monoatomic Fe_2N film. The hexagonal monatomic layer was found when the amount of the supplied N atoms was large enough. With decreasing the amount, coverage of the hexagonal monatomic layer decreases, and finally only the Fe_2N film was formed. When annealing temperature is lower than 570 K, hexagonal islands were formed (see Appendix A).

The STM measurements were performed at 77 K with a tungsten tip. Topographic images were obtained using a constant tunneling-current (I_t) mode. The tunneling spectra were recorded using a standard lock-in technique with a bias voltage (V_b) modulation of 20 mV p-p and 719 Hz. The tip-sample distance was stabilized before sweeping the bias voltage using initial set-point values of V_b and I_t. All the spectra were recorded with the same set point current 3 nA.

III. RESULTS AND DISCUSSION

A. Overlayer structure

Figure 1(a) shows a topographic image of the surface consisting of three regions with a stripe structure, the Fe_2N monoatomic film [25], and the bare Cu(001) surface. The striped regions were found nearby the step edges of the Cu(001) substrate as shown in Fig. 1(b). On each terrace, the striped region is imaged as the lowest among the three kinds of the surfaces. The topographic contrast on the same terrace comes from difference of the local density of states (LDOS), and the striped region has the lowest DOS below 0.5 eV. As we will explain later in Fig. 3, the stripe has two orientations related as mirror symmetry for the nearest neighbor directions ([110] and [$\bar{1}$10]) of the substrate Cu(001) lattice. This results in four domains of the striped surface as indicated with solid white lines in the left panel of Fig. 1(b).

In the dark area of the striped region, a hexagonal lattice illustrated with blue lines in Fig. 1(c) has an interatomic distance of 3.10 ± 0.10 Å. In the bright area another hexagonal lattice, which is marked with black lines, can be seen with a larger interatomic distance than in the dark area. As in a magnified atomically-resolved image shown in Fig. 2(a), the hexagonal protrusions result from $(\sqrt{3}\times\sqrt{3})R30^\circ$-like reconstruction of a (1×1) lattice in the bright area, which is depicted by orange lines with an average interatomic distance of 3.05 ± 0.10 Å. The same orange lattice is superimposed

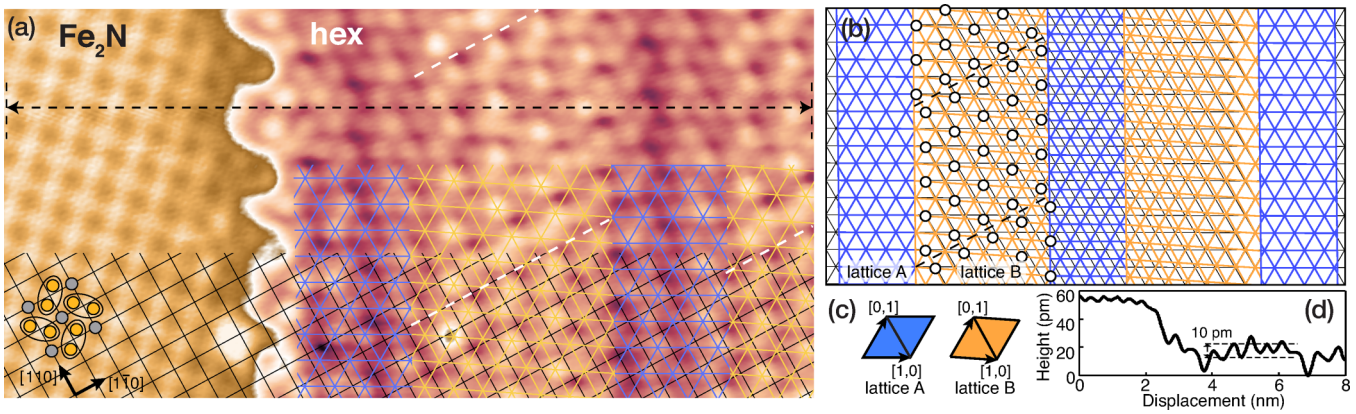

FIG. 2. (a) Atomic image of a hexagonal film and Fe_2N at $I_t = 3.0$ nA, $V_b = 0.2$ V. Black, blue, and orange solid lines correspond to lattices of underlying Cu(001), hexagonal region (lattice A), and strained hexagonal region (lattice B), respectively. White dashed lines represent phase boundaries of the $(\sqrt{3}\times\sqrt{3})R30^\circ$-like superstructure in the lattice B. Atomic configuration of Fe_2N is illustrated with a schematic model in the bottom left of the panel. In the model, orange balls are iron atoms and gray nitrogen. (b) Extracted hexagonal lattices from (a). Blue and orange lattices represent the lattice A and the lattice B, respectively. Black lattice extrapolated from the lattice A is superimposed for comparison. Atomic positions of $(\sqrt{3}\times\sqrt{3})R30^\circ$-like spots in the lattice B are represented with white circles. Dashed black lines indicate phase boundaries of the superstructure. (c) Unit vectors [1,0], [0,1] of the lattices A and B. (d) An averaged height profile along a dashed black line in (a).

on the bright area in Fig. 1(c). The superstructure contains phase boundaries every three or four periods along the stripe direction as illustrated with dashed white lines in Figs. 1(c) and 2(a). We sometimes found the "regular" region where the phase boundary repeats every three periods along the stripe direction (see Appendix B).

The two types of hexagonal lattices illustrated with blue and orange lines in Fig. 2(a) are extracted in Fig. 2(b) as "lattice A" and "lattice B." Unit cells and unit vectors of the lattices A and B are shown in Fig. 2(c). The lattice A is depicted as a perfect hexagonal lattice while the lattice B is deformed. The lattice lines along the [1,0] vector in a lattice A region show antiphase relation to the lattice lines in the next lattice A region across the lattice B region. In the whole lattice including lattice A and B, lattice lines along the [0,1] direction are shared across the domains, but the magnitude of the [0,1] vector within the lattice B is 3.5% shorter than that of lattice A, leading to surface area compressibility of 3.5% for lattice B. Moreover the [1,0] direction in lattice B is rotated 3.6° compared with that of lattice A. These can be seen by comparing lattice B with the solid black lattice extrapolated from lattice A in Fig. 2(b). The $(\sqrt{3}\times\sqrt{3})R30^\circ$-like reconstruction in lattice B is attributed to the buckling of the surface atoms due to the lattice compression. Its phase boundaries marked with dashed white lines in Figs. 1(c) and 2(a) also originate from the compression. The white circles and dashed black lines in Fig. 2(b) correspond to the $(\sqrt{3}\times\sqrt{3})R30^\circ$-like protrusions and the phase boundaries of the superstructure, respectively. Note that the compressibility of 3.5% cannot be compensated completely only by an out-of-plane displacement of the buckled atoms in lattice B. The observed buckling height ranges from 10 pm [at $V_b = 0.2$ V, Fig. 2(d)] to 20 pm [at $V_b = 3.0$ V, not shown]. The bias dependence is attributed to the increase of LDOS in the high bias regime. Since the buckling height is at most about 20 pm, apparent shrinkage against the interatomic distance of 3.1 Å due to x-y projection of the z buckling is below 0.2%. Therefore the compression in the lattice B leads to closer Fe-Fe bond length than that in the lattice A. Such ordered stripe structure consisting of two domains with different lattice strain should be made by minimizing the total strain energy [8].

B. Stacking geometry

We discuss the stacking of the hexagonal lattices on the Cu(001) lattice using the atomic image of the Fe_2N surface with a clockwised reconstruction [22,23,25] in the left side of Fig. 2(a). In a schematic model of the Fe_2N atomic structure shown in this figure, orange and gray dots correspond to Fe and N atoms, respectively. Thus, the underlying square lattice of Cu(001) in this image is depicted as shown in the bottom area of the stripe region where the model shown in Fig. 2(b) is superimposed. In the hexagonal lattices, the [1,1] and [$\bar{1}$,1] directions in both lattices A and B are closely aligned along the [1$\bar{1}$0] and [110] directions of the Cu(001) lattice, respectively. It is notable that all the atoms in the lattices A and B avoid on-top sites of the substrate Cu lattice. This leads to reduction of total strain energy and stabilizes the compressive Fe-Fe bond length in the lattice B.

Next we consider how the striped stacking configuration is realized by starting from a simple Moiré pattern made of a hexagonal sheet and a square lattice. In this model, periodicity and direction of the stripelike Moiré pattern are determined by the size and the orientation of the two lattices. First, we assume that the overlayer lattice is a perfect (free-standing) hexagonal lattice with the interatomic distance of 3.10 Å on the Cu(001) lattice with that of 2.56 Å. When one side of triangles in the hexagonal lattice is completely aligned to the [110] direction of Cu(001), defined as $\theta = 0^\circ$, the slight difference between the interatomic distance of Cu(001) and an atomic row distance of the triangle (3.10 Å$\times\sqrt{3}/2 \sim 2.68$ Å) causes a stripelike Moiré pattern shown in Fig. 3(a). In this

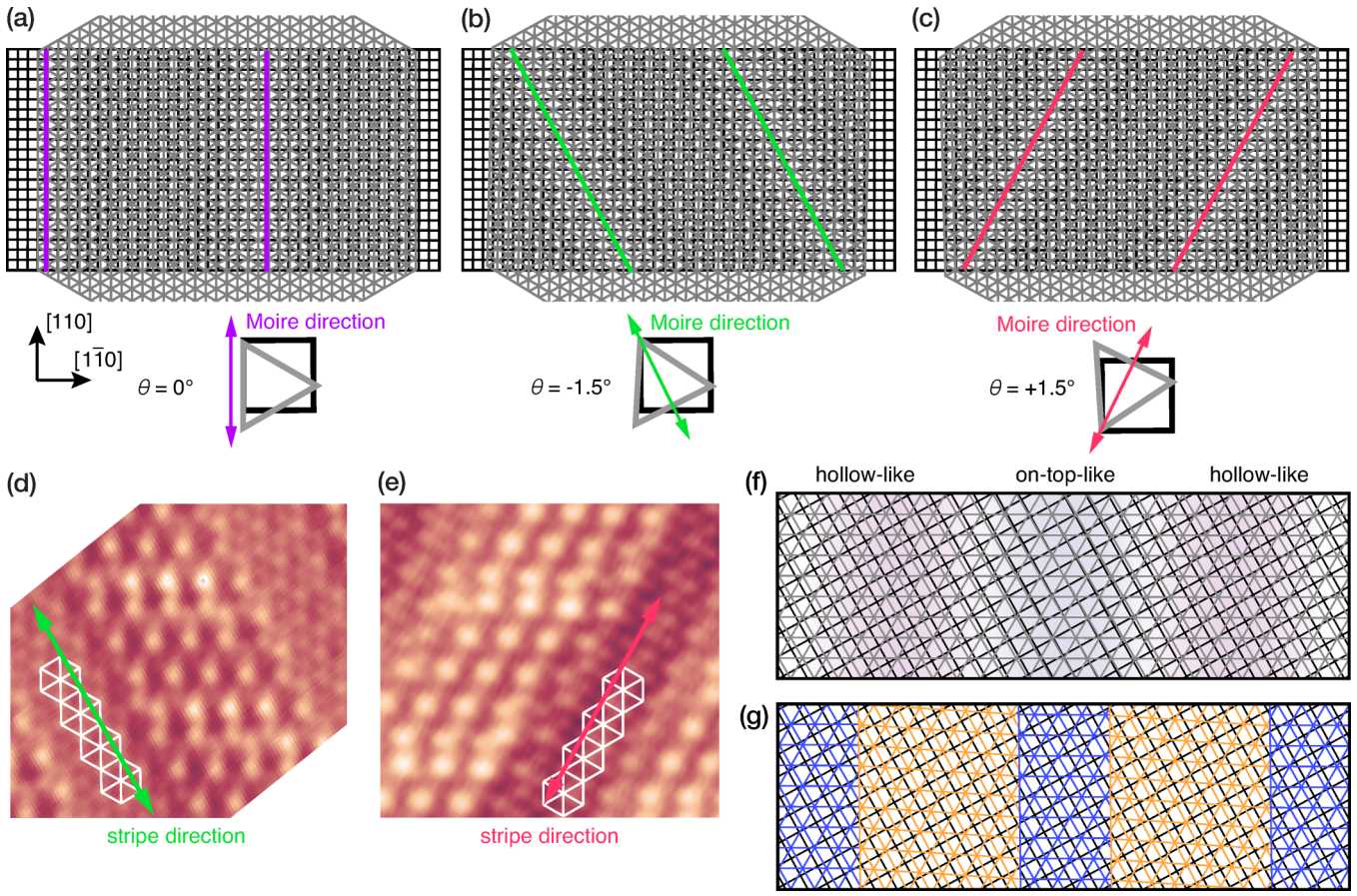

FIG. 3. (a)–(c) Moiré patterns formed between a perfect (free-standing) hexagonal lattice with the interatomic distance of 3.10 Å and the Cu(001) lattice with the interatomic distance of 2.56 Å. Rotation angle of the hexagonal lattice to Cu(001) is 0°, −1.5°, and 1.5° in (a)–(c), respectively. (d),(e) STM images of striped hexagonal films at $I_t = 1.0$ nA, $V_b = -0.1$ V. Two orientations of the stripe for lattice A (marked with white triangles) are confirmed. (f) An enlarged image of (c). (g) A superimposed image of periodically deformed hexagonal lattice of Fig. 2(b) on Cu(001). Rotation angle of the lattice A to Cu(001) is 1.5°.

case, the direction of the Moiré pattern is parallel to the [110] direction of Cu(001) and the side of the triangles in the hexagonal lattice. When the triangle is slightly tilted at $\theta = \pm 1.5°$, the Moiré direction is approximately ±30° rotated from the [110] direction of Cu(001) and almost parallel to the next-nearest-neighbor direction of the hexagonal lattice as shown in Figs. 3(b) and 3(c). These Moiré directions agree with the observed stripe directions in Figs. 3(d) and 3(e).

An enlarged image of Fig. 3(c) is depicted as in Fig. 3(f). The hexagonal lattice within both sides of the panel is located on hollow or bridge sites (hollowlike), while that within the middle region onto bridge or on-top sites (on-top-like). Then, we replace the perfect hexagonal lattice to the periodically deformed hexagonal lattice given in Fig. 2(b) while a rotation angle of the lattice A region is kept the same as that in Fig. 3(f) ($\theta = 1.5°$). The result is shown in Fig. 3(g). This model reproduces well the observed local stacking configuration in Fig. 2(a), where all the atoms avoid on-top sites of the Cu lattice. By comparing Figs. 3(f) and 3(g), it is obvious that formation of an antiphase alternation for the lattice A regions along the [1,0] direction entirely removes the on-top stacking and the deformed lattice B regions smoothly connecting the two lattice A regions also avoid the on-top stacking. Thus, the stacking in Fig. 3(g) is energetically more favorable than that in Fig. 3(f), and the same stacking relation can continue along the stripe direction. Here, we conclude that the observed stripe direction matches the Moiré direction of the model with $\theta = 1.5°$, and the periodic lattice deformation is induced to relax and stabilize the hexagonal lattice on the square Cu(001) lattice. Note that the configuration in Fig. 3(a) cannot avoid on-top stacking even with periodic in-plane deformation. The slight tilt of the hexagonal lattice is necessary to allow itself to relax onto a more stable structure with periodic strain.

C. Origin of the hexagonal lattice

We discuss a composition of the hexagonal monoatomic film. The hexagonal structure should consist of Fe and N atoms by considering the preparation process. Among bulk compounds of iron nitrides, hcp ε-Fe_3N and orthorhombic ζ-Fe_2N are classified as hexagonal-type crystals with the interatomic distances of 2.70 Å and 2.77 Å, respectively [Figs. 4(a) and 4(b)] [17,31]. Another candidate is a (111) plane of fcc γ'-Fe_4N, γ''-FeN with the ZnS structure or γ'''-FeN with the NaCl structure. Their interatomic distances are 2.68 Å, 3.06 Å, and 3.18 Å, respectively [17,26]. Considering the

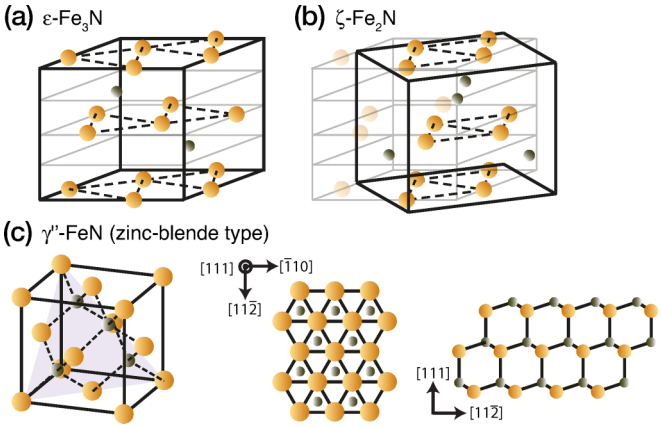

FIG. 4. Representative candidates for the observed hexagonal iron nitride. (a) ε-Fe_3N (hcp). (b) ζ-Fe_2N (orthorhombic). (c) (111) plane of γ''-FeN (ZnS structure). In all schematics orange and gray circles correspond to Fe and N atoms, respectively.

interatomic distances of 3.10 ± 0.10 Å and 3.05 ± 0.10 Å in the observed hexagonal lattices in the lattice A and B, respectively, a ZnS-type FeN is the most probable candidate [Fig. 4(c)]. We exclude the NaCl-type FeN because some theoretical calculations support that it is not stable [32]. Indeed only a ZnS-type has been reported in previous studies on epitaxial growth of FeN films [27,28].

Here, we emphasize that the strong *in-plane* Fe-N bond can allow the hexagonal lattice to be stabilized against the decomposition. Meanwhile, the periodic strain of the FeN overlayer is evidently attributed to the *interfacial* interaction between the layer and the substrate Cu(001) lattice. The whole structure of the periodically-strained hexagonal lattice can be stabilized by a delicate balance between the competing in-plane and interfacial bonds.

D. Effect of periodic strain on the electronic states

Figure 5(a) shows dI/dV spectra recorded along the dashed white line in Fig. 5(b) from the Fe_2N region to a striped region with the set point bias of 4.5 V. Figure 5(c) shows the representative spectra marked with vertical dashed lines in Figs. 5(a) and 5(b). A spectrum on the clean Cu(001) is also shown for comparison. Each spectrum on the stripe and Fe_2N surfaces exhibits a broad peak or a shoulder between 3.0 and 4.0 V. Moreover, we clearly observed that the spectral shape in the stripe region oscillates with the structural period. The spectrum changes not abruptly at the boundary between the lattices A and B, but smoothly as seen in Fig. 5(a). The spectral oscillation is also reflected in dI/dV images obtained simultaneously with topographic images at 4.20 V and 3.45 V [Figs. 5(d) and 5(e)]. Note that the spectral features in this voltage range are much more prominent than those around the Fermi level, where we could not see any feature below 2.5 V.

According to a theoretical calculation for bulk Fe_4N [33], which contains Fe_2N layers as components, its electronic structure mainly consists of N $2p$-Fe $3d$ antibonding (bonding) states around 3.5 V (−7.0 V) and other Fe $3d$ states crossing the Fermi level. For the Fe_2N monoatomic film, we previously

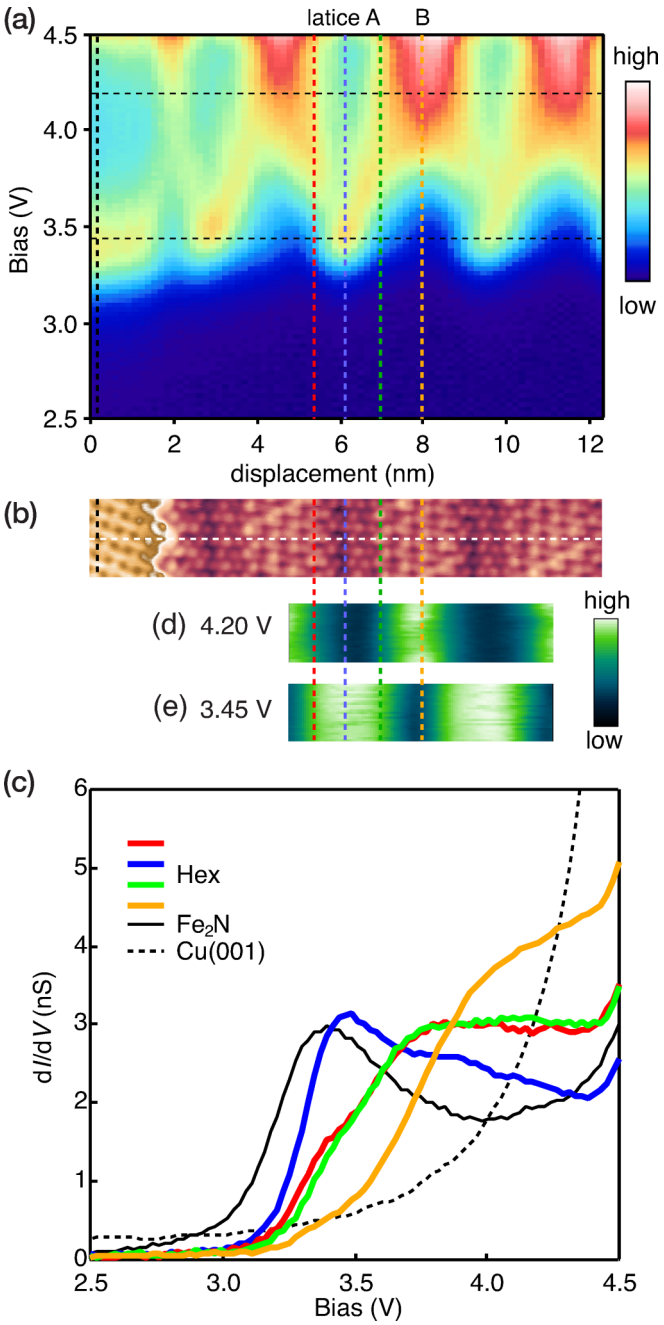

FIG. 5. Effect of periodic strain to electronic states. (a) dI/dV spectra measured along a dashed white line shown in (b) from Fe_2N (left) to a striped hexagonal film (right). Color scale corresponds to amplitude of dI/dV. Current and bias set points are $I_t = 3.0$ nA and $V_b = 4.5$ V. (b) A STM image near a boundary between Fe_2N and a striped hexagonal film. (c) Representative spectra obtained on hexagonal film and Fe_2N extracted from (a). Each color of spectra corresponds to colored vertical dashed line in (a). A comparable spectrum of Cu(001) is also presented with a dashed black line. (d),(e) dI/dV images obtained at $V_b = 4.20$ V and 3.45 V, respectively.

found peaks related to the Fe $3d$ states around the Fermi level [25], which is consistent with the calculation in Ref. [33]. Thus the broad peak in the unoccupied states of Fe_2N is identified as N $2p$-Fe $3d$ antibonding states. Such a prominent peak in unoccupied states also appears on other metal nitrides such as

strong peaks at 2.2 V and 3.9 V in an insulating Cu_2N film on Cu(001) [34–37]. Therefore, the systematic variation of the spectrum observed on the stripe region most likely originates from N $2p$-Fe $3d$ antibonding states.

Finally, we discuss the origin of the spectral oscillation in terms of strain effect. The oscillation is definitely associated with the periodic lattice strain in the hexagonal film. Generally, the lattice compression increases the atomic-orbital overlapping and widens the bandwidth for metallic systems or the band gap for semiconductors. Therefore, we conclude that the energy of the N $2p$-Fe $3d$ antibonding state is higher in the compressed lattice B than that in the expanded lattice A. Note that in our measurement we could not observe the bonding state, which was estimated to be located at -7 eV below E_F [33].

IV. SUMMARY

In summary, we synthesized monoatomic films of hexagonal iron nitride on Cu(001) and characterized them in an atomic scale using STM/STS. The hexagonal film was stabilized even on Cu(001) by the strong in-plane bonding between Fe and N atoms. The films exhibit a striped pattern consisting of strained and unstrained regions. We demonstrated that the striped structure is formed along a hypothetic Moiré direction and the periodic lattice strain is attributed to the reduction of the total lattice energy by avoiding on-top stacking on Cu(001). These indicate considerable interaction between the hexagonal film and the substrate. Furthermore we revealed that the periodic strain strongly shifts a peak in LDOS around 3.5 V. This is explained by the shift of the antibonding state due to compressive strain. Our finding suggests that the periodic strain in other types of monoatomic sheets would give further various influences to magnetic, dielectric and transport properties as well as that in electronic band structure. To stabilize the periodically strained region also in other compounds, a design of the balance between in-plane and interfacial interaction is the most important.

ACKNOWLEDGMENTS

This work was partly supported by the Japan Society for the Promotion of Science (JSPS) Grant-in-Aid for Young Scientists (A), Grant No. 16H05963, for Scientific Research (B), Grant No. 26287061, the Hoso Bunka Foundation, Shimadzu Science Foundation, and Iketani Science and Technology Foundation. Y.T was supported by the Grant-in-Aid for JSPS Fellows and the Program for Leading Graduate Schools (MERIT).

APPENDIX A: LAYERED HEXAGONAL ISLANDS AS PRECURSORS OF STRIPED HEXAGONAL FILMS

As explained in Sec. II, ordered Fe_2N monoatomic films and striped hexagonal monoatomic films are formed by annealing at 570 K after depositing Fe atoms with a large amount of N atoms on Cu(001). When the annealing temperature was as low as 540 K, we observed hexagonal-shaped islands formed around upper terraces of step edges as shown in Fig. 6(a). At this annealing temperature, the Fe_2N monatomic films are not well ordered. An enlarged image and an atomically resolved image of the hexagonal island are presented in Figs. 6(b) and 6(c), respectively. On the surface of the island we found a hexagonal lattice with an interatomic distance of 3.1 ± 0.1 Å, which is equivalent to the interatomic distance of the striped hexagonal monoatomic film formed by annealing at 570 K. The surface structure is, however, different from that of the striped hexagonal film. Thus we conclude the hexagonal island corresponds to a precursor of the striped hexagonal film.

Heights of the islands range from one to at least four layers. Figure 6(d) shows a height profile obtained at $V_b = -0.3$ V along the dashed black line in Fig. 6(b), corresponding to

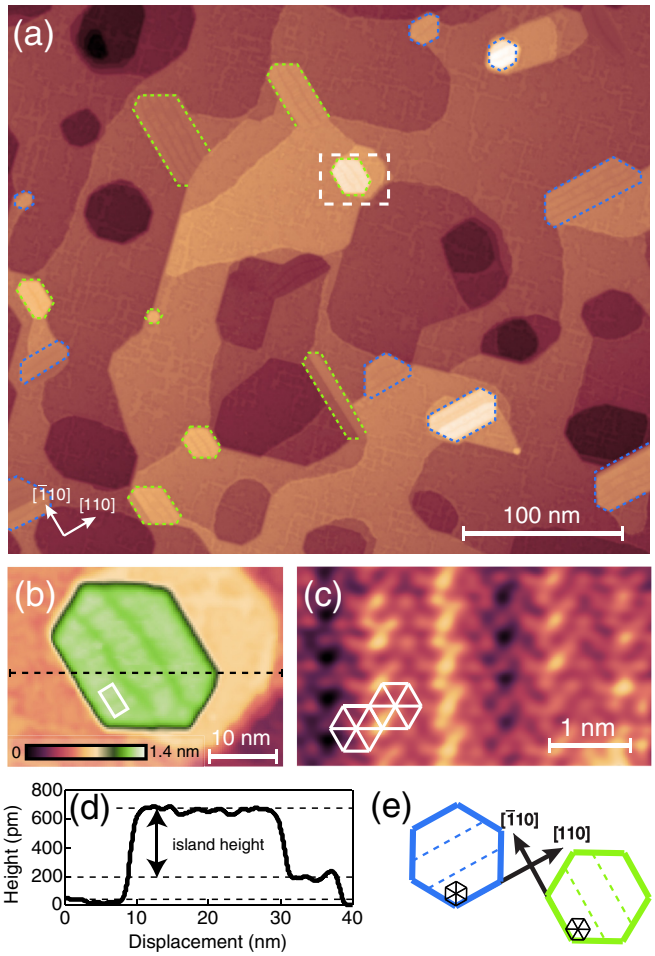

FIG. 6. A sample annealed at 540 K after N^+ ion bombardment and depositing Fe atoms. (a) An overview image of the sample obtained at $I_t = 100$ pA, $V_b = -0.3$ V. Hexagonal-shaped islands, which are indicated by dashed blue and green hexagons, were formed around upper terraces of step edges together with defected Fe_2N monoatomic films. (b) A magnified image of the dashed square in (a). (c) An atomically resolved image of the solid square in (b). A hexagonal lattice was observed on the surface of the hexagonal island. (d) A height profile along the dashed black line in (b). (e) Stacking relation between the hexagonal islands and Cu(001) substrate. Solid blue and green hexagons correspond to two types of orientation of the hexagonal island as indicated by dashed blue and green hexagons in (a).

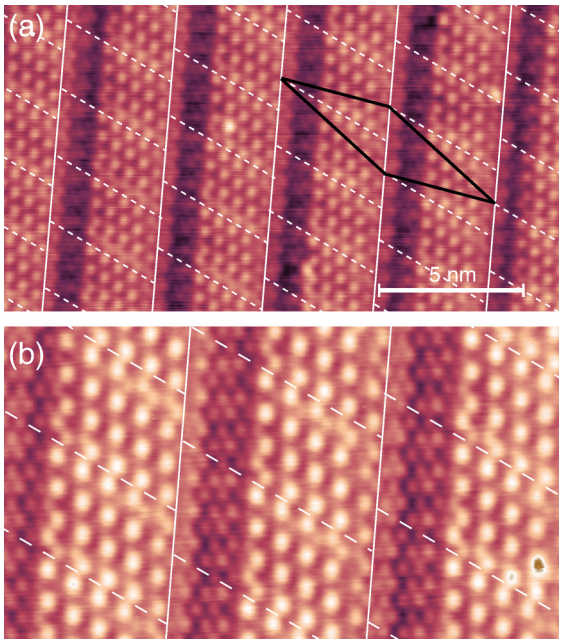

FIG. 7. (a) A "regular" striped hexagonal film, where phase boundaries in the lattice B repeat periodically along the stripe direction. Solid white lines separate striped pattern and dashed white lines indicate phase boundaries of $(\sqrt{3}\times\sqrt{3})R30^\circ$-like superstructure. A solid black parallelogram depicts a unit cell of the regular striped film. (b) An enlarged image of the regular striped region.

a double layered island. The islands exhibit two types of orientations as indicated by dashed blue and green hexagons. This suggests that a side of the hexagonal island is aligned along the nearest neighbor direction of the Cu(001) lattice in contrast to the striped hexagonal monoatomic film. Their stacking relations to Cu(001) substrate are drawn in Fig. 6(e).

APPENDIX B: REGULAR STRIPED REGION OF HEXAGONAL MONOATOMIC SHEET

In the main text, we discussed a striped hexagonal monoatomic film containing phase boundaries of $(\sqrt{3}\times\sqrt{3})R30^\circ$-like superstructure along the stripe direction every three or four periods. However we sometimes observed narrow but "regular" striped regions as shown in Figs. 7(a) and 7(b), where the phase boundaries repeated every three periods regularly. Between two adjacent rows of the regular stripe divided by solid white lines phase boundaries show antiphase configuration. The direction of the regular stripe structure slightly differs from that of the "irregular" ones shown in the main text (approximately 5° rotated from next-nearest-neighbor direction of the lattice A), suggesting that the stacking geometries to Cu(001) are also different. This narrow region was surrounded partly by upper step edges, and thus the substrate could be deformed differently from that at a large terrace.

[1] G. H. Olsen, C. J. Nuese, and R. T. Smith, J. Appl. Phys. **49**, 5523 (1978).
[2] H. Asai and K. Oe, J. Appl. Phys. **54**, 2052 (1983).
[3] T. P. Pearsall, F. H. Pollak, J. C. Bean, and R. Hull, Phys. Rev. B **33**, 6821 (1986).
[4] C. G. Van de Walle and R. M. Martin, Phys. Rev. B **34**, 5621 (1986).
[5] P. F. Carcia, A. D. Meinhaldt, and A. Suna, Appl. Phys. Lett. **47**, 178 (1985).
[6] P. Krams, F. Lauks, R. L. Stamps, B. Hillebrands, and G. Güntherodt, Phys. Rev. Lett. **69**, 3674 (1992).
[7] J. Giergiel, J. Shen, J. Woltersdorf, A. Kirilyuk, and J. Kirschner, Phys. Rev. B **52**, 8528 (1995).
[8] K.-O. Ng and D. Vanderbilt, Phys. Rev. B **52**, 2177 (1995).
[9] P. Merino, M. Švec, A. L. Pinardi, G. Otero, and J. A. Martín-Gago, ACS Nano **5**, 5627 (2011).
[10] M. Corso, W. Auwärter, M. Muntwiler, A. Tamai, T. Greber, and J. Osterwalder, Science **303**, 217 (2004).
[11] A. T. N'Diaye, S. Bleikamp, P. J. Feibelman, and T. Michely, Phys. Rev. Lett. **97**, 215501 (2006).
[12] A. B. Preobrajenski, M. L. Ng, A. S. Vinogradov, and N. Mårtensson, Phys. Rev. B **78**, 073401 (2008).
[13] A. L. Vázquez de Parga, F. Calleja, B. Borca, M. C. G. Passeggi, Jr., J. J. Hinarejos, F. Guinea, and R. Miranda, Phys. Rev. Lett. **100**, 056807 (2008).
[14] B. Wang, M. Caffio, C. Bromley, H. Früchtl, and R. Schaub, ACS Nano **2**, 1487 (2008).
[15] S. J. Altenburg and R. Berndt, New J. Phys. **16**, 053036 (2014).
[16] H. Kim and Y. Hasegawa, Phys. Rev. B **93**, 075409 (2016).
[17] J. M. D. Coey and P. A. I. Smith, J. Magn. Magn. Mater. **200**, 405 (1999).
[18] C. M. Fang, M. A. van Huis, J. Jansen, and H. W. Zandbergen, Phys. Rev. B **84**, 094102 (2011).
[19] Y. Hashimoto, K. Nakatsuji, T. Iimori, and F. Komori, Surf. Sci. **604**, 451 (2010).
[20] X. Liu, B. Lu, T. Iimori, K. Nakatsuji, and F. Komori, Phys. Rev. Lett. **98**, 066103 (2007).
[21] H. A. Wriedt, N. A. Gokcen, and R. H. Nafziger, Bull. Alloy Phase Diagrams **8**, 355 (1987).
[22] J. M. Gallego, S. Y. Grachev, D. M. Borsa, D. O. Boerma, D. Écija, and R. Miranda, Phys. Rev. B **70**, 115417 (2004).
[23] J. M. Gallego, D. O. Boerma, R. Miranda, and F. Ynduráin, Phys. Rev. Lett. **95**, 136102 (2005).
[24] Y. Takagi, K. Isami, I. Yamamoto, T. Nakagawa, and T. Yokoyama, Phys. Rev. B **81**, 035422 (2010).
[25] Y. Takahashi, T. Miyamachi, K. Ienaga, N. Kawamura, A. Ernst, and F. Komori, Phys. Rev. Lett. **116**, 056802 (2016).
[26] H. Nakagawa, S. Nasu, H. Fujii, M. Takahashi, and F. Kanamaru, Hyp. Int. **69**, 455 (1992).
[27] W. Lin, J. Pak, D. C. Ingram, and A. R. Smith, J. Alloys Compd. **463**, 257 (2008).
[28] C. Navio, J. Alvarez, M. J. Capitan, F. Yndurain, and R. Miranda, Phys. Rev. B **78**, 155417 (2008).

[29] V. Higgs, P. Hollins, M. E. Pemble, and J. Pritchard, J. Electron Spectrosc. Relat. Phenom. **39**, 137 (1986); S. M. Driver and D. P. Woodruff, Surf. Sci. **442**, 1 (1999).
[30] H. Baek, S. Jeon, J. Seo, and Y. Kuk, J. Kor. Phys. Soc. **56**, 620 (2010).
[31] K. H. Jack, Acta Crystallogr. **5**, 404 (1952).
[32] P. Lukashev and W. R. L. Lambrecht, Phys. Rev. B **70**, 245205 (2004).
[33] M. Sifkovits, H. Smolinski, S. Hellwig, and W. Weber, J. Magn. Magn. Mater. **204**, 191 (1999).
[34] C. D. Ruggiero, T. Choi, and J. A. Gupta, Appl. Phys. Lett. **91**, 253106 (2007).
[35] K. Bhattacharjee, X.-D. Ma, Y. Q. Zhang, M. Przybylski, and J. Kirschner, Surf. Sci. **606**, 652 (2012).
[36] J. C. Oberg, M. R. Calvo, F. Delgado, M. Moro-Lagares, D. Serrate, D. Jacob, J. Fernández-Rossier, and C. F. Hirjibehedin, Nat. Nanotechnol. **9**, 64 (2014).
[37] Ruggiero *et al.*, have claimed the two possible assignments: (i) the peak at 2.2 V corresponds to the onset of conduction band consisting of N $2p$-Cu $3d$ antibonding state and that at 3.9 V is due to the nitrogen p_z orbital, (ii) the peak at 2.2 V is due to an interfacial state between Cu_2N and Cu(001) and that at 3.9 V reflects the onset of the conduction band. Oberg *et al.*, have followed (i).